JCTC Journal of Chemical Theory and Computation

Article

pubs.acs.org/JCTC

Performance and Accuracy of Recursive Subspace Bisection for Hybrid DFT Calculations in Inhomogeneous Systems

William Dawson* and François Gygi*

Department of Computer Science, University of California Davis, Davis, California 95616, United States

ABSTRACT: The high cost of computing the Hartree−Fock exchange energy has resulted in a limited use of hybrid density functionals in solid-state and condensed phase calculations. Approximate methods based on the use of localized orbitals have been proposed as a way to reduce this computational cost. In particular, Boys orbitals (or maximally localized Wannier functions in solids) were recently used in plane wave, first-principles molecular dynamics simulations of water. Recently, the recursive subspace bisection (RSB) method was used to compute orbitals localized in regular rectangular domains of varying shape and size, leading to efficient calculations of the Hartree−Fock exchange energy in the plane-wave, pseudopotential framework. In this paper, we use the RSB decomposition to analyze orbital localization properties in inhomogeneous systems (e.g., solid/liquid interfaces) in which localized orbitals have widely varying extent. This analysis reveals that some orbitals cannot be significantly localized and thus cannot be truncated without incurring a substantial error in computed physical properties, while other orbitals can be well localized to small domains. We take advantage of the ability to systematically reduce the error in RSB calculations through a single parameter to study the effect of orbital truncation. We present the errors in PBE0 ground state energies, ionic forces, band gaps, and relative energy differences between configurations for a variety of systems, including a tungsten oxide/water interface, a silicon/water interface, liquid water, and bulk molybdenum. We show that the RSB approach can adapt to such diverse configurations by localizing orbitals in different domains while preserving a 2-norm upper bound on the truncation error. The resulting approach allows for efficient hybrid DFT simulations of inhomogeneous systems in which the localization properties of orbitals vary during the course of the simulation.

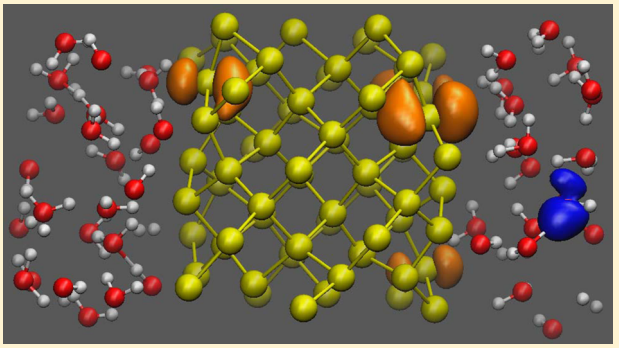

1. INTRODUCTION

Electronic structure calculations based on density functional theory (DFT) have been very successful in predicting the properties of a wide variety of condensed-matter systems.[1,2] The accuracy of DFT calculations depends critically on the choice of exchange and correlation functional used. Typical choices are the local-density approximation (LDA) or one of many generalized gradient approximation (GGA) functionals[3] which provide good computational efficiency and relatively good accuracy, in particular for covalently bonded solids.[4] Most LDA and GGA functionals however are insufficiently accurate to describe weakly bonded systems, such as molecular liquids and van der Waals complexes, often leading to overbinding of molecules.[3] This deficiency has led several authors to propose new density functionals that take into account the effect of dispersion interactions or van der Waals forces[5−7]

Furthermore, LDA and GGA functionals fail to properly include the long-range nonlocal Hartree−Fock exchange interaction, which is expected to be significant in semiconductors and insulators. Hybrid density functionals,[8,9] such as e.g. B3LYP,[10,11] PBE0,[12] and HSE,[13] were introduced in order to improve these approximations by including in their definition a fraction of the Hartree−Fock exchange energy

$$E_x^{\mathrm{HF}} = -\frac{1}{2}\sum_{i,j=1}^{N}\int_{\mathrm{BZ}} \mathrm{d}q\mathrm{d}q' \int \frac{\phi_{iq}^*(r)\phi_{jq'}^*(r)\phi_{jq'}(r')\phi_{iq}(r')}{|r-r'|}\mathrm{d}r\mathrm{d}r' \tag{1}$$

where ϕ are Kohn−Sham orbitals, i,j denote the band index, q,q' are wave vectors in the Brillouin zone, and N is the number of occupied bands. In solids, hybrid density functionals have been shown to improve the accuracy of computed lattice constants, bulk moduli, and band gap energies.[14−16] Hybrid DFT molecular dynamics simulations of liquid water have also shown substantial improvements in vibrational spectra compared with GGA simulations.[17]

The computational cost of hybrid DFT calculations is usually dominated by the cost of the evaluation of Hartree−Fock exchange. When using localized basis functions, this cost can be reduced considerably by exploiting the localization properties of the basis functions, reducing the nominal cost of $O(N^4)$ to $O(N)$.[18−21] If extended basis functions are used (e.g., plane waves), the cost of Hartree−Fock exchange can only be reduced to $O(N^2M \log M)$ using fast Fourier transforms (FFT) (where M is the number of points in the FFT grid). Note that

Received: June 18, 2015

DOI: 10.1021/acs.jctc.5b00826
J. Chem. Theory Comput. XXXX, XXX, XXX−XXX

in dense systems, $M \propto N$, so that the cost scales as $O(N^3 \log N)$. In spite of this high cost, the use of the plane wave basis remains attractive in condensed systems since its translational invariance eliminates basis set superposition errors (BSSE) and facilitates energy-conserving first-principles molecular dynamics simulations.

In semiconductors and insulators, the cost of Hartree−Fock exchange can be further reduced by exploiting the localization properties of orbitals. Kohn's "near-sightedness" principle[22] ensures that Kohn−Sham orbitals can be transformed into orbitals exhibiting exponential localization, if the HOMO−LUMO gap is finite. This property has been used to simplify the computation of Hartree−Fock exchange by using Boys orbitals[23] (or equivalently, maximally localized Wannier functions (MLWF))[24,25] and, in another approach, by using a recursive subspace bisection (RSB) of the Kohn−Sham orbitals.[26] We discuss these two approaches and their applicability to various systems in more detail in the next section.

In this paper, we use the RSB decomposition to analyze orbital localization properties in various systems, including inhomogeneous systems (e.g., solid/liquid interfaces) in which localized orbitals have widely varying extent. We find that some orbitals cannot be significantly localized and thus cannot be truncated without incurring a substantial error in computed physical properties. We compute PBE0 ground state energies, ionic forces, and HOMO−LUMO gaps and show that, by systematically reducing the bisection threshold parameter, the error in those quantities can be arbitrarily reduced in a controlled way, while preserving a significant acceleration of the computation. We find that the performance and accuracy of the method is preserved in inhomogeneous systems in which orbitals exhibit variable degrees of localization.

Section 2 includes a discussion of orbital localization methods and compares the RSB approach with the MLWF approach. Sections 3-7 include an analysis of the accuracy of our approach. We discuss the performance of the method in Section 8. The use of RSB as an analysis tool is discussed in Section 9. Finally, we present our conclusions in Section 10.

2. ORBITAL LOCALIZATION METHODS

The solutions of the Kohn−Sham equations can be described as a subspace spanned by a set of orbitals that minimize the Kohn−Sham energy. Any orthogonal transformation among such orbitals also represents a valid and equivalent solution. Localization methods take advantage of this extra degree of freedom by choosing an orthogonal transformation that yields localized orbitals. Depending on the choice of localization criterion, various schemes lead to different localized orbitals.[27,28] Boys orbitals[23] (or Maximally Localized Wannier functions (MLWFs)) are obtained by minimizing the spatial spread of orbitals in real space.[29]

Localized orbitals can be used to accelerate calculations by selectively avoiding computations involving nonoverlapping orbitals and additionally by computing some integrals in a limited volume. In particular, the computation of the Hartree−Fock exchange energy can be accelerated by neglecting exchange integrals for pairs of orbitals localized in well separated regions.

2.1. Maximally Localized Wannier Functions. Calculations of Hartree−Fock exchange based on MLWFs were proposed by Wu et al.[30] In that approach, exchange integrals are selected on the basis of a fixed, chosen cutoff radius. MLWFs associated with Wannier centers separated by a distance larger than this radius are neglected. This approach was shown to work well in liquid water, a system in which all Wannier functions have similar extent. In that case, a single cutoff radius is used to select pairs of orbitals based on the distance between Wannier centers. This cutoff radius is chosen by trial and error, until a satisfactory accuracy is obtained for the computed energy and ionic forces. Wu et al. compute exchange integrals for each selected pair of orbitals by solving a Poisson equation in a spherical subdomain of the real-space grid where the two orbitals of the pair are localized. Another fixed cutoff radius is chosen to determine the size of the spherical domain in which the Poisson equation is solved. Skipping exchange integrals involving nonoverlapping MLWFs reduces the cost of Hartree−Fock exchange to $O(N^2 \log N)$ when using the plane wave basis. In addition, the calculation of the exchange integral in a limited domain further reduces the cost to $O(N \log N)$. The size of the truncation domains must be chosen a priori, and the error resulting from the truncation may vary and must be tested a posteriori. This approach relies on the assumption that the radii of the truncation domains can be determined in advance. If, however, the MLWFs exhibit variable degrees of localization, or if their localization varies during the simulation, the approach is less straightforward and requires an adaptive algorithm which has so far not been demonstrated.

Many systems of interest are, however, inhomogeneous, i.e. their MLWFs are localized on domains of varying size. This is in particular the case in systems including different materials with different electronic properties, e.g. semiconductor−insulator interfaces, water-semiconductor interfaces, or solvated semiconducting nanoparticles. Furthermore, the computation of some electronic properties (e.g., the HOMO−LUMO gap) requires the calculation of both occupied and unoccupied orbitals. The localization properties of occupied and unoccupied orbitals can be very different, even in a homogeneous system such as liquid water, as will be discussed below. In such situations, the use of a fixed cutoff radius for the selection of exchange orbitals is impractical and would likely lead to overconservative selection criteria if accuracy is to be preserved.

2.2. Recursive Subspace Bisection. The recursive subspace bisection method (RSB)[31] provides an alternative method for the localization of orbitals. In that approach, Kohn−Sham orbitals are transformed into orbitals localized in rectangular domains of various sizes and shapes, while guaranteeing an upper bound in the 2-norm error caused by the truncation of orbitals in these domains. The error bound is chosen a priori by specifying the RSB threshold, while the size and shape of the localization domains are an outcome of the calculation. The main advantage of the RSB procedure is that no information regarding the achievable degree of localization of orbitals must be known in advance. The use of RSB localization results in a reduction of the cost of Hartree−Fock exchange to $O(N^2 \log N)$ if exchange integrals are computed in the entire computational domain. Reducing the integration domain to the overlap of the localization domains would reduce the cost further to $O(N \log N)$, as in the MLWF-based approach.

Although this last step would lower the cost of the Hartree−Fock exchange calculation, we have chosen to avoid it and compute the exchange integrals for each pair in the entire simulation domain. The cost of exchange remains $O(N^2 \log N)$,

DOI: 10.1021/acs.jctc.5b00826
J. Chem. Theory Comput. XXXX, XXX, XXX−XXX

but, as an important corollary, the variational principle is preserved, i.e. the error in the exchange energy due to the use of a finite RSB threshold is positive. As a consequence, the convergence of the calculation with respect to the value of the RSB threshold can be meaningfully analyzed, since lowering the RSB threshold is guaranteed to lower the total energy. An important feature of this approach is that the bisection threshold can be reduced continuously to zero, in which case the full exchange calculation is performed, without other approximations. If spherical domains are used to compute exchange integrals, the variational principle is not guaranteed, and the convergence analysis is not straightforward. Furthermore, the radius of the spherical domain cannot be simply increased until the exact integral is computed, due to overlap of the domain with periodic replicas.

The RSB method[26,31] relies on the definition of a set of projectors P^k onto subdomains Ω_k of the simulation domain (see the Appendix). The projector P^k acts on orbitals by truncating them to the domain Ω_k. The symmetric matrices representing these projectors in the subspace of occupied orbitals are simultaneously diagonalized using an approximate simultaneous diagonalization procedure, which generates an orthogonal transformation to localized orbitals. Choosing projectors P^k to be Walsh projectors, we can generate a set of orbitals that are localized on a hierarchy of rectangular domains of varying size. Using this method, we can bound the 2-norm of the projection onto the subdomains

$$\int_{\Omega_k} |P^k \phi_i(r)|^2 \mathrm{d}r \geq (c_i^k)^2 \tag{2}$$

where c_i^k is the singular value of the projector P^k on orbital i. This provides a natural way to control the error caused by truncation of an orbital on a subdomain. We choose a threshold value ϵ and truncate orbital i on Ω_k if $1 - (c_i^k)^2 \leq \epsilon$. This truncation procedure leads to a large reduction in the number of exchange integrals that must be computed to evaluate the Hartree−Fock exchange energy. Since the error introduced by skipping an exchange integral is positive (from the sign in eq 1), convergence can be attained by reducing the value of ϵ. The degree of localization of orbitals varies and is related to the HOMO−LUMO gap.[32] We observed that, in some systems, a substantial number of orbitals can be localized even when the HOMO−LUMO gap is small.

While both the MLWF and RSB methods provide a significant speedup in the calculation of the exchange energy and offer some control over the error, none of them offers an easy-to-calculate *a priori* bound on the error in the energy or ionic forces. The parameters, e.g. the RSB threshold in the RSB approach or the spheres' radii in the MLWF approach, must be adjusted empirically until an acceptable error is found. This is the approach taken by DiStasio et al.[33] using MLWFs. In the case of the RSB method, Gaiduk et al.[34] and Wan et al.[35] determined an appropriate RSB threshold by comparing first-principles MD simulations performed with various threshold values. Little is known so far about the transferability of such parameters to different physical systems, and some sensitivity analysis will likely remain a necessity. However, the RSB approach is appealing in this context: it only includes a single parameter, which is associated with a physical quantity (the amount of charge density being truncated for each orbital), and preserves the variational principle. We find empirically that the RSB threshold is a good indicator of the error in computed physical quantities and that it is likely transferable between different systems. In the rest of this paper, we systematically evaluate the error due to orbital truncation for systems showing a variety of localization properties. These results can serve as a guideline for choosing parameters in future calculations.

3. ORBITAL LOCALIZATION IN INHOMOGENEOUS SYSTEMS

We assess the performance and accuracy of the RSB approach by applying it to various inhomogeneous systems exhibiting different properties, notably regarding the localization properties of orbitals. The systems considered are (a) a 128-molecule liquid water sample, (b) a tungsten oxide/water interface represented by 64 WO_3 formula units arranged in a slab and surrounded by 72 water molecules (see Figure 1), (c) a silicon/water interface including a slab of 64 silicon atoms surrounded by 44 water molecules (see Figure 2), and (d) bulk molybdenum represented by the BCC two-atom primitive cell (lattice parameter a = 5.94698 au) replicated four times in each direction (128 atoms). For systems (a-c), we compute the ground state energy and ionic forces in configurations extracted from molecular dynamics simulations performed at finite temperature. System (d) (bulk Mo) represents a special type of "inhomogeneous" system in which different energy bands exhibit different localization properties. As will be described below, the Mo 4*s* and 4*p* semicore orbitals can be well localized (in spite of the system being metallic), whereas the 4*d*−5*s* orbitals remain extended.

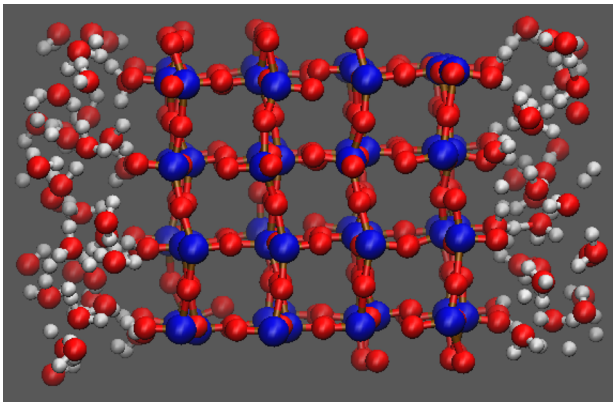

Figure 1. Tungsten oxide/water interface.

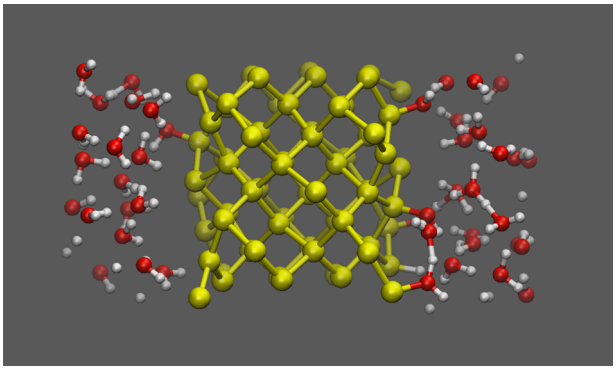

Figure 2. Silicon/water interface.

We also analyze the accuracy of the method on an ensemble of 32 configurations of a 64-molecule liquid water system.

DOI: 10.1021/acs.jctc.5b00826
J. Chem. Theory Comput. XXXX, XXX, XXX−XXX

These configurations were taken from 32 independent PBE simulations of 58 ps each, ensuring that configurations are uncorrelated. This ensemble allows us to study the relative energies of various configurations and ensure that reaction pathways and system relaxations are preserved when using the RSB approach.

We use the RSB approach as implemented in the Qbox code,[36] with 3×3×3 bisection levels. Electron−ion interactions are represented using norm-conserving pseudopotentials.[37,38] For bulk molybdenum, we use the Optimized Norm-Conserving Vanderbilt pseudopotentials of Schlipf et al.[39]

The ground state energy of each of these systems was calculated using the PBE0 hybrid functional. In systems (a-c) we chose a plane wave energy cutoff of 85 Ry. For system (d) we use a plane wave energy cutoff of 60 Ry. The corresponding FFT grid sizes are given in Table 1. Ground state energy values

Table 1. Size of the FFT Grids Used in the Calculations

parameter	value
H_2O	180 × 180 × 180
WO_3/H_2O	176 × 180 × 288
Si/H_2O	128 × 128 × 256
bulk Mo	128 × 128 × 128

were converged to within 10^{-8} (au), and forces were converged to within 10^{-6} (au). Reference values for the energy and forces were first calculated without the RSB approximation (i.e., with a threshold value $\epsilon = 0$). We then computed the PBE0 ground state energy using the RSB approximation with various threshold values, starting from randomized orbitals.

The choice of the above systems was motivated by their different properties in terms of localization of orbitals and spatial inhomogeneity. It was found by several authors[40] that orbitals in liquid water (system (a)) can be readily localized using MLWFs. As we show below, the presence of another system (e.g., WO_3 or Si) can dramatically change the localization properties of orbitals.

As a measure of the localization of orbitals, we define the *pair fraction* as the number of orbital pairs selected for the computation of the exchange energy, divided by the total number of orbital pairs. The pair fraction depends on the RSB threshold ϵ. In the limit $\epsilon \to 0$, the pair fraction approaches 1. For finite values of ϵ, the pair fraction gives a direct measure of the reduction in the cost of the exchange energy calculation. The pair fraction of systems (a-d) is shown in Table 2 for various values of ϵ. The pair fraction gradually approaches 1 as the threshold decreases, which allows for a systematic improvement of the accuracy.

Systems (a-c) all have very low pair fractions, which translates into good performance improvement. However, system (d) has a large pair fraction (≈0.7) even at the highest threshold value, indicating that electronic states cannot be localized effectively. Further analysis shows that the electronic

Table 2. Pair Fraction after Bisection

ϵ	H_2O	WO_3/H_2O	Si/H_2O	bulk Mo
0.001	0.369	0.414	0.837	0.998
0.005	0.145	0.084	0.508	0.960
0.01	0.083	0.059	0.379	0.820
0.02	0.049	0.047	0.202	0.757
0.05	0.025	0.031	0.097	0.719

states associated with the 4*d*−5*s* band cannot be localized, while semicore orbitals (4*s* and 4*p*) can be localized effectively to small domains. This system therefore shows unique localization properties in which different bands have different localization properties. If a larger supercell is used (e.g., by replicating the system in one direction), some of the 4*d*−5*s* orbitals can be localized, leading to a decrease of the pair fraction to about 0.4, as shown in Table 3. The achievable pair fraction remains

Table 3. Pair Fraction vs Unit Cell Size in Bulk Mo for a Threshold $\epsilon = 0.05$[a]

cell size	N_{atoms}	pair fraction
4 × 4 × 4	128	0.719
4 × 4 × 6	192	0.661
4 × 4 × 8	256	0.591
4 × 4 × 10	320	0.555
4 × 4 × 12	384	0.505
4 × 4 × 14	448	0.422

[a]The cell size denotes the multiplication factors used to replicate the BCC 2-atom unit cell in the *x*, *y*, and *z* directions.

however rather large, indicating that controlled truncation of orbitals in such a system only allows for a limited speedup. This example illustrates how, even in the case of a bulk metal, the RSB approach allows one to identify orbitals that can be localized and make optimal use of localization properties.

A more fine-grained way to look at the different localization properties of these systems consists in computing for each orbital the fraction of the domain occupied by its localized representation. This quantity is shown in Figure 3 for a threshold value of 0.05.

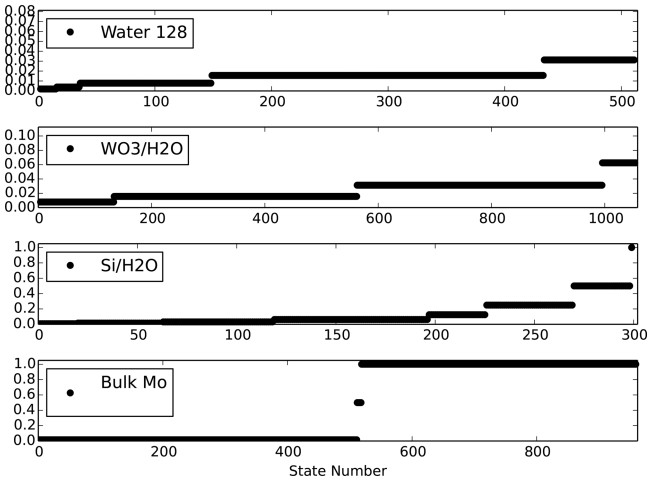

Figure 3. Fraction of the domain occupied by each localized orbital for a threshold $\epsilon = 0.05$. Note the different scales for each system.

These values reveal the unique localization properties of each system. Orbitals in pure liquid water can be localized very well, with all orbitals localized within at most 3% of the unit cell. However, even in pure water, we find that certain orbitals localize better than others. In the tungsten oxide/water interface, orbitals associated with water molecules are localized quite similarly to those in liquid water, while the orbitals associated with the tungsten oxide region are much more extended. We also observe a wide variety of localization properties in the silicon/water interface, where some orbitals

DOI: 10.1021/acs.jctc.5b00826
J. Chem. Theory Comput. XXXX, XXX, XXX−XXX

remain relatively delocalized, even to the extent that a single orbital remains completely delocalized throughout the domain. Even though the bulk molybdenum system is composed of only one type of atom, its orbitals localize in an inhomogeneous fashion. The 4*s* and 4*p* orbitals localize tightly around each atom, while the other (4*d*−5*s*) orbitals remain almost completely delocalized (with a few localizing into half of the domain). These results illustrate the various classes of localization that can be achieved in inhomogeneous systems using the RSB approach. In all cases, the 2-norm error caused by truncation of an orbital to its localization domain is bounded by the threshold ϵ. Such inhomogeneous systems are representative of a broad class of condensed matter systems that we wish to study with hybrid functionals.

4. ENERGY ERROR

We have computed the error in the ground state energy obtained using RSB in systems (a-d). The error is defined as the difference in the total energy of a system computed with RSB and without RSB. We report in Table 4 the difference in the total energy. Note that the difference in total energy is not equal to the difference in exchange energy, since self-consistency induces a small change in other energy terms.

Table 4. Error in the Total Energy (au) for Various Values of the Threshold ϵ

ϵ	H_2O	WO_3/H_2O	Si/H_2O	bulk Mo
0.001	1.11×10^{-3}	5.64×10^{-3}	3.51×10^{-4}	1.4×10^{-6}
0.005	1.47×10^{-2}	1.10×10^{-1}	7.05×10^{-3}	4.81×10^{-3}
0.01	3.78×10^{-2}	1.54×10^{-1}	1.82×10^{-2}	3.72×10^{-1}
0.02	1.01×10^{-1}	2.14×10^{-1}	8.84×10^{-2}	6.74×10^{-1}
0.05	2.20×10^{-1}	8.02×10^{-1}	2.48×10^{-1}	9.76×10^{-1}

Comparing energy errors, we see that the silicon/water interface has the lowest error of all systems for thresholds 0.01 and 0.02. For smaller threshold values (0.005 and 0.001), bulk molybdenum has the smaller error. On the other hand, the tungsten oxide/water interface consistently has the largest error. These trends can be attributed to system size (300 vs 1056 occupied orbitals in Si/H_2O and WO_3/H_2O, respectively). Since truncation is done on each orbital, it is expected that the energy error will be proportional to the number of orbitals. Table 5 shows normalized values of the energy error, i.e. the error per orbital.

Table 5. Energy Error (au) per Orbital

ϵ	H_2O	WO_3/H_2O	Si/H_2O	bulk Mo
0.001	2.28×10^{-6}	5.34×10^{-6}	1.17×10^{-6}	7.8×10^{-10}
0.005	2.87×10^{-5}	1.04×10^{-4}	2.35×10^{-5}	2.68×10^{-5}
0.01	7.39×10^{-5}	1.46×10^{-4}	6.08×10^{-5}	2.07×10^{-4}
0.02	1.98×10^{-4}	2.03×10^{-4}	2.95×10^{-4}	3.76×10^{-4}
0.05	4.31×10^{-4}	7.60×10^{-4}	8.28×10^{-4}	5.45×10^{-4}

When considering normalized errors, we find that the difference between the smallest and largest error across systems is consistently contained within a factor of 2−5 except at 0.001 for bulk molybdenum which has a pair fraction extremely close to 1. The error remains relatively close among systems with a variety of localization properties, depending primarily on the choice of threshold. Even though bulk molybdenum has many delocalized orbitals, the error from localization is comparable to systems that localize very well. The error correlates with the threshold, and not the pair fraction value, which means that a user does not need to consider whether orbitals of a given system will localize better. This data can be used as a guide in the choice of an appropriate threshold value for other systems, as the error depends more on the threshold value than the properties of the particular system considered.

5. ERRORS IN FORCES

While the results in the previous section provide guidance for controlling the energy error and demonstrate the systematic convergence of RSB, the error in the energy remains high in absolute terms. For example, reducing the energy error to 10^{-8} (au) would require a very small threshold value, which would then negate the benefit of using a localization approach. In the following, we provide evidence that the energy error consists mostly of an additive term which does not affect the structure and dynamics of the system. Such a systematic additive error can be compared e.g. to the change in energy observed when improving the quality of a basis set. For example, Halkier et al.[41] found a difference in energy in a water dimer of 1.0759×10^{-2} (au) when going from a triple-ζ to quadruple-ζ basis set. Scaling this value to 128 molecules (system (a)), this basis set change could thus introduce an error as large as 7×10^{-1} (au), which is larger than that observed with the 0.05 threshold value. Similarly to what is observed in the case of basis set improvement, we expect the RSB energy error to be additive and mostly constant in different atomic configurations.

Analyzing the error in atomic forces provides further evidence that the error introduced by the RSB procedure is a systematic additive term. We have computed the error in atomic forces for systems (a-c) obtained using RSB. The maximum error is recorded in Table 6, and the average error is recorded in Table 7. These results show that the errors in forces can be reduced to acceptable levels for molecular dynamics simulations and for structure optimization with moderate values of the threshold. They also show a good correlation between force errors and the threshold values. Halving the threshold leads to approximately halving the error in the forces. This, combined with the fact that the force errors are very similar across systems, shows that we can likely use this data to predict the error in forces in other systems. The small errors observed

Table 6. Maximum Absolute Force Error (au)

ϵ	H_2O	WO_3/H_2O	Si/H_2O
0.001	7.70×10^{-5}	9.10×10^{-5}	8.40×10^{-5}
0.005	1.05×10^{-3}	1.80×10^{-3}	5.37×10^{-4}
0.01	1.52×10^{-3}	3.08×10^{-3}	1.12×10^{-3}
0.02	5.40×10^{-3}	5.11×10^{-3}	3.80×10^{-3}
0.05	8.09×10^{-3}	1.05×10^{-2}	7.89×10^{-3}

Table 7. Average Absolute Force Error (au)

ϵ	H_2O	WO_3/H_2O	Si/H_2O
0.001	9.0×10^{-6}	1.1×10^{-5}	1.0×10^{-5}
0.005	6.4×10^{-5}	2.6×10^{-4}	6.4×10^{-5}
0.01	1.5×10^{-4}	3.6×10^{-4}	1.2×10^{-4}
0.02	3.9×10^{-4}	5.0×10^{-4}	3.5×10^{-4}
0.05	8.1×10^{-4}	1.4×10^{-3}	9.5×10^{-4}

DOI: 10.1021/acs.jctc.5b00826
J. Chem. Theory Comput. XXXX, XXX, XXX−XXX

in the forces indicate that the error in the energy is mostly independent of atomic positions and can therefore be considered a constant additive term.

6. ERRORS IN HOMO–LUMO GAPS

We have computed the PBE0 band gap using various values of the RSB threshold in order to analyze the effect of RSB truncation on band gap values. A total of 64 unoccupied orbitals were included in the calculations in each system considered. Additional care must be taken in the simultaneous diagonalization procedure when unoccupied orbitals are present. The diagonalization algorithm must be modified to prevent mixing of occupied and unoccupied orbitals.[26]

The RSB procedure is able to localize even high-energy unoccupied orbitals. Similar to Figure 3, Figure 4 shows the

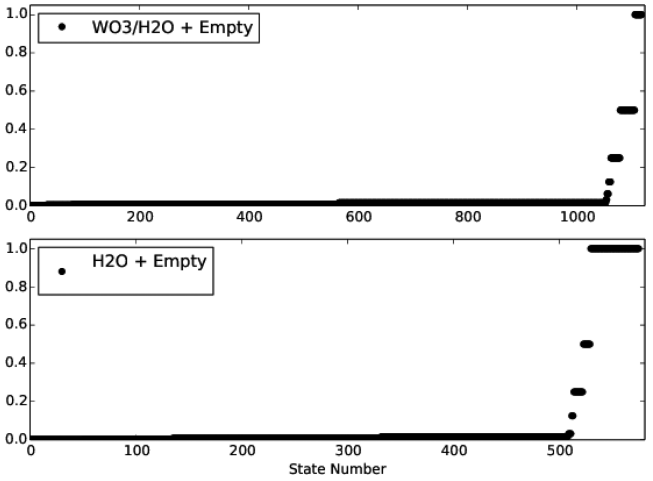

Figure 4. Portion of the domain occupied by each localized orbital for a threshold $\epsilon = 0.05$, including unoccupied orbitals.

portion of the unit cell occupied by localized orbitals. After RSB is performed, many unoccupied orbitals are localized nearly as well as occupied orbitals. However, others are only localized on one-half or one-quarter of the unit cell, and a few remain completely delocalized. As with the silicon/water, interface, the RSB procedure is able to handle the full range of localization properties.

The ground state energy and band gap of the tungsten oxide/water interface and of the liquid water system were computed self-consistently at various threshold levels. Figure 5 shows isosurface representations of the absolute value of the valence band maximum (VBM) and conduction band minimum (CBM) orbitals in the tungsten oxide/water interface. At all threshold levels, these orbitals are localized on the same side of the tungsten oxide slab. Note that in some cases, the orbitals of the VBM and CBM may be localized on opposite sides of the slab depending on the atomic configuration at a particular time step in a simulation. The band gap values are reported in Table 8. Figure 5 shows that the VBM and CBM orbitals are localized in the vicinity of one surface of the slab but are extended in directions parallel to the interface. For these orbitals, truncation in a small region would likely lead to inaccurate results. The RSB approach identifies partially extended orbitals (for the chosen treshold), thus avoiding their truncation to small domains.

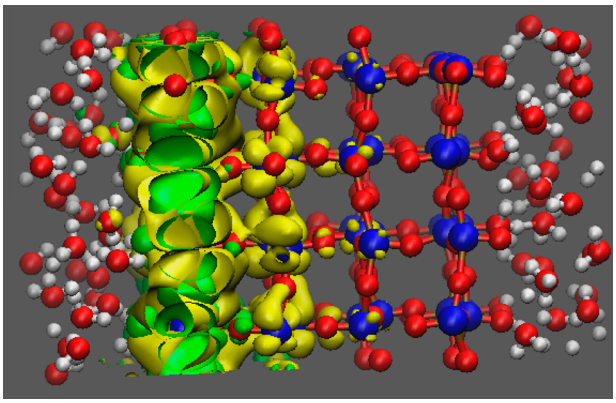

Figure 5. Isosurfaces of the absolute value of the VBM (yellow) and CBM (green) orbitals in the tungsten oxide/water interface.

Table 8. Band Gap of Liquid Water and of the Tungsten Oxide/Water Interface (eV) at Various Threshold Levels

ϵ	H_2O	WO_3/H_2O
0.0	6.43	3.96
0.001	6.43	3.96
0.005	6.42	3.88
0.01	6.42	3.86
0.02	6.40	3.85
0.05	6.36	3.84

7. ERRORS IN RELATIVE ENERGIES

We now consider in more detail relative energy differences between different configurations of a single system. Such differences are important in the study of reaction pathways or when determining the lowest energy structure of a system. If the RSB procedure is to be applied in these studies, it is important that relative energy values between configurations are preserved. We consider here the 32 configurations of 64-molecule water samples described in section 3.

For each configuration of water, the PBE0 ground state was calculated using various RSB threshold levels. We then sorted the configurations based on their energy computed *without* using RSB. The energy values are plotted in Figure 6. In this figure, a strictly decreasing line indicates that the relative energy ordering is preserved despite the use of RSB.

Figure 6 shows that up to a threshold of 0.02 the relative energy ordering is well preserved. Furthermore, up to a threshold of 0.01 the shape of the line looks extremely similar

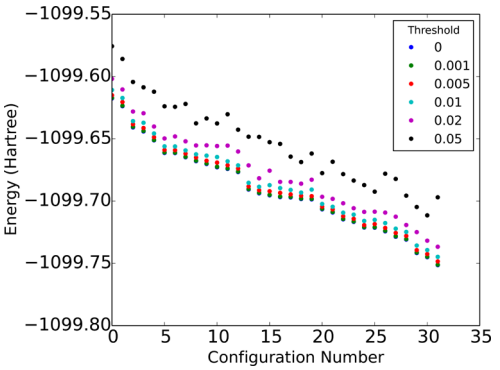

Figure 6. Total energy (au) for each configuration sorted by the energy values when no RSB is used.

DOI: 10.1021/acs.jctc.5b00826
J. Chem. Theory Comput. XXXX, XXX, XXX–XXX

to the exact result, apart from a constant upward shift in energy (Figure 7). This provides evidence that the error introduced by the use of RSB is mostly an additive constant.

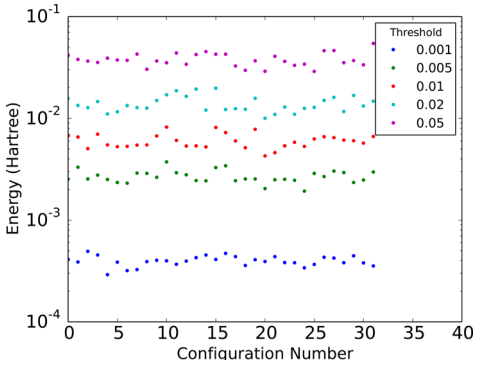

Figure 7. Log plot of the difference in energy (au) between a configuration at a certain threshold and the energy of a configuration with no RSB.

The histograms in Figure 8 provide another view of the error introduced by RSB. For each configuration, we calculated the

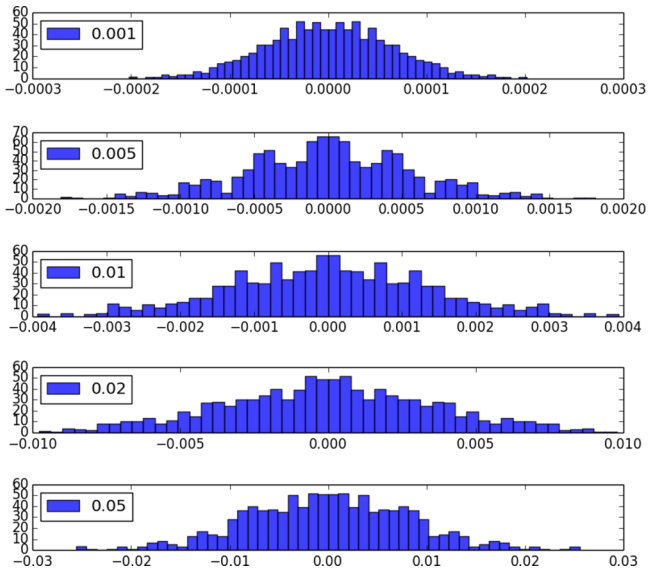

Figure 8. Distribution of the error in energy differences (au) between configurations using various RSB thresholds.

difference in energy between that configuration and all other configurations. We then subtracted that energy difference at a given threshold from the value obtained without RSB and binned the values in a histogram. Note that the horizontal scale in the figure varies with threshold value. The lower the threshold value, the higher the resolution of the energy differences between configurations. With a threshold of 0.01, the error is well contained within 4×10^{-3} (au). We can compare this value to the basis set superposition error (BSSE) observed in atom-centered basis set computations. Halkier et al.[41] found that the counterpoise correction to the binding energy of a single water dimer amounts to 4.82×10^{-5} (au) using an aug-cc-pVQZ basis set. Multiplying this error by 32 to compare with our 64-molecule system would yield a total counterpoise correction of approximately 2×10^{-3} (au). Thus, the relative error introduced with a 0.01 RSB threshold is comparable in magnitude to the error incurred from basis set superposition errors when using atom centered basis sets at the aug-cc-pVQZ level.

8. PERFORMANCE

The choice of the bisection threshold results from a trade-off between performance and accuracy. In the previous sections, we provided reference values for the accuracy of RSB on various systems. In this section, we focus on the performance and scalability of the calculations.

Performance data was obtained using the Qbox code on the Mira BlueGene/Q computer at Argonne National Laboratory. We used the IBM XL compiler with an O3 level of optimization and the appropriate tuning options for the BlueGene/Q platform. We use four MPI tasks per node with four threads per task. We take advantage of the mixed MPI/threading model by using threaded linear algebra libraries and OpenMP threads for the 3D Fourier transforms and in other numerically intensive parts of the code. The reported wall-clock times refer to one PBE0 self-consistent (SCF) iteration. The number of SCF iterations needed to complete a Born−Oppenheimer iteration depend on many other parameters which we do not include in this analysis.

Tables 9 and 10 show the performance data for the liquid water and silicon/water interface, respectively. A threshold of at least 0.01 is needed for significant speedup. Performance scales well up to 8,192 cores for the silicon/water interface and 16,384 cores for liquid water.

Table 9. Time per SCF Step (s) for the Liquid Water System for Various Threshold Values

cores	0.05	0.02	0.01	0.005	0.001	no bisection
2,048	11.6	17.1	24.5	37.7	80.8	291.0
4,096	8.4	11.5	15.8	22.7	45.1	149.1
8,192	4.9	6.8	9.3	13.4	26.6	89.8
16,384	3.4	4.4	5.8	8.0	15.3	49.5
32,768	3.3	4.1	5.2	7.2	13.2	42.2

Table 10. Time per SCF Step (s) for the Silicon/Water Interface for Various Threshold Values

cores	0.05	0.02	0.01	0.005	0.001	no bisection
2,048	10.8	17.6	27.9	35.5	54.6	77.3
4,096	7.6	11.0	16.3	20.0	29.5	39.6
8,192	3.9	5.8	8.6	10.8	16.1	21.3
16,384	3.7	5.3	7.6	9.3	13.6	18.3

The tungsten oxide/water interface is larger than the other systems considered, both in terms of unit cell volume and number of orbitals. This offers more opportunities for the localization of orbitals, and thus better performance and better scalability at low threshold values. The performance data is shown in Table 11. A significant speedup can be seen even at a threshold as low as 0.001, and performance scales well up to 64k cores.

9. RSB AS A TOOL TO ANALYZE ORBITAL LOCALIZATION PROPERTIES

The consistency in error demonstrated across a variety of systems demonstrates that the 2-norm criterion for truncation used by RSB is a good measure to consider a function localized. This makes RSB a useful tool for further analyzing and

DOI: 10.1021/acs.jctc.5b00826
J. Chem. Theory Comput. XXXX, XXX, XXX−XXX

Table 11. Time per SCF Step (s) for the Tungsten Oxide/Water Interface for Various Threshold Values

cores	0.05	0.02	0.01	0.005	0.001	no bisection
4,096	48.0	63.0	73.5	95.3	364.3	1039.2
8,192	26.8	34.9	40.6	52.2	195.4	592.8
16,384	22.7	27.6	31.0	38.0	118.3	390.1
32,768	14.5	17.5	19.6	23.8	72.3	205.4
65,536	12.7	14.5	15.8	18.3	47.5	116.2

comparing the localization properties of different systems and their relation to other physical properties. For example, the existence of a localized orbital representation has been empirically associated with the presence of a gap in the Kohn−Sham eigenvalue spectrum. Our results show that in some systems in which the HOMO−LUMO gap is small (e.g., Si/H_2O), a large fraction of orbitals may be still be localized in small domains. In the case of bulk molybdenum, the RSB decomposition shows that a large number of orbitals can be localized, even though the system is metallic. This suggests that the presence of a band gap may not be the only relevant criterion for the existence of localized orbitals. Beyond its use in accelerating the evaluation of the Hartree−Fock exchange energy, the RSB decomposition can also be used to determine how much data compression can be achieved when representing a wave function within a given error tolerance. This could prove useful in devising new algorithms for higher-order perturbation methods or for efficient quantum Monte Carlo computations.

The Qbox code[36] implements the RSB decomposition through the `bisection` command, which can be used as a standalone feature to compute localized orbitals. The command reports the portion of the domain each orbital is localized in. It also yields orbitals in a localized representation, which can be subjected to further analysis and visualization.

10. CONCLUSION

Using the recursive subspace bisection method to localize orbitals in an inhomogeneous condensed system can dramatically reduce the cost of computing Hartree−Fock exchange while preserving a controlled error. In this work, we have used the ability to systematically reduce the error of the RSB approximation through a single parameter and analyzed the error introduced in representative inhomogeneous condensed systems for a variety of threshold values. We have shown that errors in the energy per orbital remain within an order of magnitude across a variety of systems at the same threshold level. We have also shown that errors in the forces are small and can be systematically reduced by reducing the threshold. Errors in the energy appear to be mostly due to an additive constant that does not affect relative energy differences. Our results also show that the RSB decomposition is a useful tool to analyze the localization properties of orbitals in a wide range of systems. Because our conclusions are derived from systems exhibiting a variety of localization properties, our data also serves as a reference for future calculations involving the RSB approximation. We have also provided data on the performance of these calculations using a variety of partition sizes on the Mira BlueGene/Q computer. This data shows a large speedup due to the use of RSB that remains scalable up to 32k cores even for moderate-sized systems. The RSB approximation involves a trade off between performance and accuracy, and the values provided in this work serve as a guide in the choice of threshold level most appropriate for hybrid DFT simulations.

APPENDIX

We outline here the main steps involved in computing the RSB decomposition. A detailed description of the RSB approach is given in ref 31. In the first step, a set of projectors P^k must be chosen. The simplest choice (one bisection level) consists of three square-wave functions P^x, P^y, P^z having a value of 1 in one-half of the unit cell and 0 in the other half, along the x, y, and z directions, respectively. The symmetric matrices A^k associated with these projectors are defined as

$$a_{ij}^k = \int \phi_i(r) P^k \phi_j(r) \mathrm{d}r \tag{3}$$

and are computed by forming the corresponding products on the real-space Fourier transform grid. A simultaneous diagonalization of the matrices A^k is then performed using the algorithm of Cardoso and Souloumiac.[42] Note that the matrices A^k do not commute in general and can therefore not be simultaneously diagonalized exactly. The Cardoso-Souloumiac algorithm provides the orthogonal transformation that makes the matrices A^k maximally diagonal. The diagonal elements of the matrices after diagonalization provide the values $(c_i^k)^2$ used in eq 2. When using multiple levels of bisection, projectors are added in the form of additional square-wave functions appropriately staggered along the x, y, and z directions (Walsh functions). This leads to a larger set of symmetric matrices A^k, which must all be (approximately) simultaneously diagonalized. The resulting set of values $(c_i^k)^2$ is then used to determine in which subdomain the orbital i is localized.

AUTHOR INFORMATION

Corresponding Authors

*E-mail: wddawson@ucdavis.edu.

*E-mail: fgygi@ucdavis.edu.

Notes

The authors declare no competing financial interest.

ACKNOWLEDGMENTS

This work is supported by the U.S. Department of Energy Office of Basic Energy Sciences through grant DE-SC0008938. Allocation of computing resources by NSF XSEDE through the award TG-ASC090004 is gratefully acknowledged. An award of computer time was provided by the DOE Innovative and Novel Computational Impact on Theory and Experiment (INCITE) program. This research used resources of the Argonne Leadership Computing Facility at Argonne National Laboratory, which is supported by the Office of Science of the U.S. Department of Energy under contract DE-AC02-06CH11357. This research used resources of the National Energy Research Scientific Computing Center, a DOE Office of Science User Facility supported by the Office of Science of the U.S. Department of Energy under Contract No. DE-AC02-05CH11231. Figures 1, 2, and 5 were generated using the VMD software.[43]

REFERENCES

(1) Dreizler, R. M.; Gross, E. K. U. *Density Functional Theory: An Approach to the Quantum Many-Body Problem*; Springer: 1990.

(2) Martin, R. M. *Electronic Structure. Basic Theory and Practical Methods*; Cambridge University Press: 2004.

DOI: 10.1021/acs.jctc.5b00826
J. Chem. Theory Comput. XXXX, XXX, XXX−XXX

(3) Becke, A. D. J. *J. Chem. Phys.* **2014**, *140*, 18A301.
(4) Haas, P.; Tran, F.; Blaha, P.; Schwarz, K.; Laskowski, R. *Phys. Rev. B: Condens. Matter Mater. Phys.* **2009**, *80*, 195109.
(5) Dion, M.; Rydberg, H.; Schröder, E.; Langreth, D. C.; Lundqvist, B. I. *Phys. Rev. Lett.* **2004**, *92*, 246401.
(6) Tkatchenko, A.; Scheffler, M. *Phys. Rev. Lett.* **2009**, *102*, 073005.
(7) Klimeš, J.; Bowler, D. R.; Michaelides, A. *Phys. Rev. B: Condens. Matter Mater. Phys.* **2011**, *83*, 195131.
(8) Burke, K. *J. Chem. Phys.* **2012**, *136*, 150901.
(9) Becke, A. D. *J. Chem. Phys.* **1993**, *98*, 1372−1377.
(10) Becke, A. D. *J. Chem. Phys.* **1993**, *98*, 5648−5652.
(11) Lee, C.; Yang, W.; Parr, R. G. *Phys. Rev. B: Condens. Matter Mater. Phys.* **1988**, *37*, 785−789.
(12) Adamo, C.; Barone, V. *J. Chem. Phys.* **1999**, *110*, 6158−6170.
(13) Heyd, J.; Scuseria, G. E.; Ernzerhof, M. *J. Chem. Phys.* **2003**, *118*, 8207−8215.
(14) Paier, J.; Marsman, M.; Hummer, K.; Kresse, G.; Gerber, I. C.; Ángyn, J. G. *J. Chem. Phys.* **2006**, *125*, 249901.
(15) Janesko, B. G.; Henderson, T. M.; Scuseria, G. E. *Phys. Chem. Chem. Phys.* **2009**, *11*, 443−454.
(16) Heyd, J.; Scuseria, G. E.; Ernzerhof, M. *J. Chem. Phys.* **2003**, *118*, 8207.
(17) Zhang, C.; Donadio, D.; Gygi, F.; Galli, G. *J. Chem. Theory Comput.* **2011**, *7*, 1443.
(18) Schwegler, E.; Challacombe, M. *J. Chem. Phys.* **1996**, *105*, 2726−2734.
(19) Schwegler, E.; Challacombe, M.; Head-Gordon, M. *J. Chem. Phys.* **1997**, *106*, 9708−9717.
(20) Ochsenfeld, C.; White, C. A.; Head-Gordon, M. *J. Chem. Phys.* **1998**, *109*, 1663−1669.
(21) Izmaylov, A. F.; Scuseria, G. E.; Frisch, M. J. *J. Chem. Phys.* **2006**, *125*, 104103.
(22) Kohn, W. *Phys. Rev. Lett.* **1996**, *76*, 3168−3171.
(23) Boys, S. F. *Rev. Mod. Phys.* **1960**, *32*, 296−299.
(24) Marzari, N.; Vanderbilt, D. *Phys. Rev. B: Condens. Matter Mater. Phys.* **1997**, *56*, 12847−12865.
(25) Wu, X.; Selloni, A.; Car, R. *Phys. Rev. B: Condens. Matter Mater. Phys.* **2009**, *79*, 085102.
(26) Gygi, F.; Duchemin, I. *J. Chem. Theory Comput.* **2013**, *9*, 582−587.
(27) Edmiston, C.; Ruedenberg, K. *Rev. Mod. Phys.* **1963**, *35*, 457.
(28) Marzari, N.; Vanderbilt, D. *Phys. Rev. B: Condens. Matter Mater. Phys.* **1997**, *56*, 12847.
(29) Marzari, N.; Mostofi, A. A.; Yates, J. R.; Souza, I.; Vanderbilt, D. *Rev. Mod. Phys.* **2012**, *84*, 1419.
(30) Wu, X.; Selloni, A.; Car, R. *Phys. Rev. B: Condens. Matter Mater. Phys.* **2009**, *79*, 085102.
(31) Gygi, F. *Phys. Rev. Lett.* **2009**, *102*, 166406.
(32) Prodan, E.; Kohn, W. *Proc. Natl. Acad. Sci. U. S. A.* **2005**, *102*, 11635−11638.
(33) DiStasio, R. A., Jr; Santra, B.; Li, Z.; Wu, X.; Car, R. *J. Chem. Phys.* **2014**, *141*, 084502.
(34) Gaiduk, A. P.; Zhang, C.; Gygi, F.; Galli, G. *Chem. Phys. Lett.* **2014**, *604*, 89−96.
(35) Wan, Q.; Spanu, L.; Gygi, F.; Galli, G. *J. Phys. Chem. Lett.* **2014**, *5*, 2562−2567.
(36) http://qboxcode.org (accessed Aug 25, 2015).
(37) Hamann, D.; Schlüter, M.; Chiang, C. *Phys. Rev. Lett.* **1979**, *43*, 1494.
(38) Vanderbilt, D. *Phys. Rev. B: Condens. Matter Mater. Phys.* **1985**, *32*, 8412.
(39) Schlipf, M.; Gygi, F. *Comput. Phys. Commun.* **2015**, *196*, 36.
(40) Silvestrelli, P. L.; Parrinello, M. *Phys. Rev. Lett.* **1999**, *82*, 3308−3311.
(41) Halkier, A.; Klopper, W.; Helgaker, T.; Jo, P.; Taylor, P. R. *J. Chem. Phys.* **1999**, *111*, 9157−9167.
(42) Cardoso, J.-F.; Souloumiac, A. *SIAM journal on matrix analysis and applications* **1996**, *17*, 161−164.
(43) Humphrey, W.; Dalke, A.; Schulten, K. *J. Mol. Graphics* **1996**, *14*, 33−38.

DOI: 10.1021/acs.jctc.5b00826
J. Chem. Theory Comput. XXXX, XXX, XXX−XXX